OXFORD

Journal of Geophysics and Engineering

Journal of Geophysics and Engineering (2020) **17**, 838–851 doi:10.1093/jge/gxaa033

Filtering of a Ricker wavelet induced by anelastic seismic wave propagation and reflection

Stephan Ker [1,*] **and Yves Le Gonidec** [2]

[1] IFREMER, Géosciences Marines, Centre de Brest, 29280 Plouzané, France
[2] Univ Rennes, CNRS, Géosciences Rennes, UMR 6118, 35000 Rennes, France

[*] Corresponding author: Stephan Ker. E-mail: stephan.ker@ifremer.fr

Received 9 April 2020, revised 28 May 2020
Accepted for publication 17 June 2020

Abstract

A varying Q factor with depth induces modifications of seismic wave features due to anelastic propagation but also reflections at the discontinuities. Standard signal analysis methods often neglect the reflection contribution when assessing Q values from seismic data. We have developed an analytical quantification of the cumulative effects of both the propagation and reflection contributions by considering Kjartansson's model and a seismic plane wave at normal incidence on a step-like discontinuity. We show that the cumulative effects are equivalent to a frequency filter characterised by a bandform and phase that both depend on the ratio between the elastic and anelastic contrasts. When considering this filter applied to a Ricker wavelet, we establish an analytical expression of the peak-frequency attribute as a function of propagation and reflection properties. We demonstrate that this seismic attribute depends on the anelastic contrast, which cannot be neglected when assessing Q factors: the error in Q estimate is not linearly dependent on the anelastic contrast and we establish an analytical expression for the case where this contrast is weak. An unexpected phenomenon for a step-like interface is an increase in the peak frequency that is observed when the anelastic and elastic contrasts have opposite signs, with a constraint on the anelastic propagation properties. This behaviour allows for assessment of the elastic and anelastic parameters.

Keywords: seismic attenuation, Q factor, anelasticity, seismic data analysis

1. Introduction

In the framework of exploration seismology, wave propagation in attenuating media has been extensively studied to understand amplitude loss, frequency content reduction and phase distortion induced by anelastic processes (Kolsky 1956; Futterman 1962; Toksöz & Johnston 1981). Over the last decades, intensive research efforts have been dedicated to the quantification of seismic attenuation through the estimate of the quality factor Q (Dasgupta & Clark 1998; Reine *et al.* 2009; Tary *et al.* 2017), the attenuation compensation of seismic data through Q-inverse filtering methods (Wang 2002, 2008), Q compensation in migration (Wang 2008a; Dutta & Schuster 2014; Zhu *et al.* 2014; Li *et al.* 2016) and seismic inversion (Causse *et al.* 1999; Innanen & Lira 2010; Brossier 2011; Innanen 2011). Most of these studies focused on the attenuation effects on a seismic wave during its propagation in an anelastic medium, which can be characterised by a Q factor varying with depth. However, it has been shown that Q-contrast effects may also affect the seismic wave during its reflection by an anelastic reflector (White 1965; Bourbié & Nur 1984; Lines *et al.* 2014). This contribution is commonly neglected in analytical modelling. Developing quantitative analyses that takes into account the effect of anelastic propagation and reflection contributions on seismic waves remains of first-order importance in the understanding and exploitation of reflected seismic

data. Currently, frequency-dependent seismic anomalies observed on seismic data have been attributed to strong absorptive reflection coefficients associated with contrasts of both P-wave velocities and Q factor properties between two layers (Chapman *et al.* 2006; Odebeatu *et al.* 2006; Ker *et al.* 2014; Wu *et al.* 2015). In particular, the P- and Q-contrasts are negative/negative or positive/negative for seismic reflectors associated with carbonate reservoirs (Adam *et al.* 2009; Takam Takougang & Bouzidi 2018), rocks saturated with heavy oil (Gurevich *et al.* 2008) and hydrate bearing sediments (Guerin & Goldberg 2005; Marin-Moreno *et al.* 2017). To explain such absorptive reflection coefficients (Castagna *et al.* 2003), different mechanisms can be considered in the framework of anelastic, i.e. viscoelastic (Lam *et al.* 2004; Borcherdt 2009; Zhao *et al.* 2018) or poroelastic (Chapman *et al.* 2006; Quintal *et al.* 2009) wave propagation.

In the case of anelastic interfaces, White (1965) introduced the concept of absorptive reflection and Bourbié & Nur (1984) experimentally identified pure anelastic reflection respectively associated with a Q-contrast between two anelastic layers. Lines *et al.* (2014) confirmed these observations by developing innovative laboratory experiments. The motivation in studying anelastic reflections, related to the imaginary part of the complex seismic impedance controlled by the quality factor (White 1965; Lines *et al.* 2008; Morozov 2011), is better interpreting reflected wave amplitude (Bourbié & Nur 1984) and phase rotation (Lines *et al.* 2014). But these studies do not deal with an anelastic upper layer, i.e. anelastic propagation is not considered before the reflection and the impact of the Q-contrast magnitude on the reflected wave is still not quantified. A full understanding of the impact of both anelastic propagation and reflection on an incoming seismic wave has not been provided yet and constitutes the aim of this work.

We develop an analytical analysis to quantify the cumulative effects of both the propagation and reflection contributions by considering Kjartansson's model and a seismic plane wave at normal incidence on a step-like discontinuity. In section 2, we review the anelastic seismic wave propagation and reflection associated with the constant-Q model (Kjartansson 1979) that is widely used in seismic modelling, inversion and analysis (Morgan *et al.* 2012; Chen *et al.* 2018; Ker *et al.* 2019) and we revisit these wave phenomena in terms of frequency filtering. We develop a comprehensive analysis by introducing new constitutive parameters, related to both propagation and reflection. In section 3, we present the filter related to the cumulative effects of both anelastic propagation and reflection and describe its frequency behaviour. In section 4, we investigate the effect of this cumulative filter on a seismic source signal approximated by a Ricker wavelet and develop analytical descriptions of peak-frequency parameters to quantify the wavelet shape distortions induced by the cumulative filter. This investigation provides some insights and pitfalls related to the use of the peak-frequency attribute when estimating Q values or interpreting seismic data.

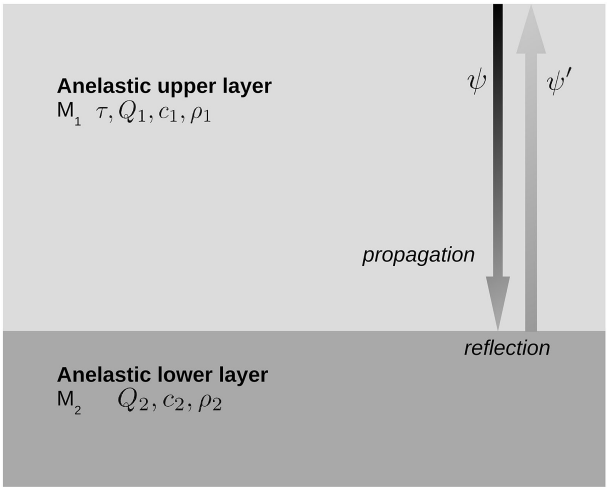

Figure 1. Step-like reflector defined by two homogeneous anelastic layers: an anelastic propagation of a normal plane incoming wave in the upper layer and an anelastic reflection of the wave at the discontinuity.

2. Frequency filters associated with anelastic propagation and reflection

2.1. *Principles of the approach*

We assume a 1D plane-wave seismic propagation and a step-like reflector defined between two anelastic layers M_1 and M_2 (figure 1). As a consequence, a reflected seismic wave ψ' is the result of two contributions induced on the incoming wave ψ, *i.e.* (i) a propagation in the upper anelastic layer and (ii) a reflection at the anelastic interface. To develop a quantitative analysis of these effects, our proposed method consists of defining frequency filters (bandform and phase) associated with these two contributions in terms of both modulus and phase expressed in the frequency domain.

2.2. *Modulus and phase associated with the anelastic propagation contribution*

Seismic propagation occurs in the upper anelastic layer M_1 characterised by a density ρ_1, a reference velocity c_1 and a quality factor Q_1. The attenuation quantified by Q_1 induces a complex P-wave velocity $v_1^*(\omega)$, which depends on the angular frequency ω of the seismic wave. Based on Kjartansson's model (Kjartansson 1979), $v_1^*(\omega)$ can be expressed as a function of Q_1 and c_1 according to:

$$v_1^*(\omega) = c_1 \left(\frac{\omega}{\omega_h}\right)^{\frac{1}{\pi}\arctan\frac{1}{Q_1}} \left[1 - i\tan\left(\frac{1}{2}\arctan\frac{1}{Q_1}\right)\right]^{-1}, \quad (1)$$

where the reference angular frequency ω_h ensures the compliance with the Kramers–Kröning dispersion relation and corresponds to the highest frequency of the seismic source frequency content (Wang & Guo 2004; Wang 2008b). In the following, we consider the approximate form of the complex velocity:

$$v_1^*(\omega) \simeq c_1 \left(\frac{\omega}{\omega_h}\right)^{\frac{1}{\pi Q_1}} \left[1 + \frac{i}{2Q_1}\right], \tag{2}$$

which induces an error lower than 1.5% for a quality factor larger than 5. According to this approximation, the phase velocity and attenuation associated with the real and imaginary parts of the complex wavenumber $k_1^* = \omega / v_1^*(\omega)$, respectively, can be used to highlight that the anelastic propagation acts as a filter defined by the modulus $M_p(\omega) = \exp(-\frac{\omega\tau}{2Q_1})$ and the phase $P_p(\omega) = \tau\omega(1 - (\frac{\omega}{\omega_h})^{-\frac{1}{\pi Q_1}})$ where τ is the travel time in the upper anelastic layer M_1.

By introducing the ratio:

$$\Gamma = \frac{4Q_1}{\pi\tau}, \tag{3}$$

which has the dimension of a frequency, and assuming $\pi Q_1 >> 1$, we can finally write:

$$M_p(\omega) = \exp\left(-\frac{2\omega}{\pi\Gamma}\right), \tag{4a}$$

$$P_p(\omega) = \frac{4\omega}{\pi^2\Gamma} \ln\left(\frac{\omega}{\omega_h}\right), \tag{4b}$$

which highlights that the anelastic propagation in the upper layer acts as a filter that depends on the frequency parameter Γonly. This means that the filter related to the anelastic propagation is unchanged when both the travel time and the attenuation proportionally increase or decrease.

The frequency response of the filter associated with wave propagation in the upper anelastic layer is described by the partial derivatives of both the modulus and phase with respect to the angular frequency ω. This is given as:

$$\frac{\partial M_p(\omega)}{\partial\omega} = -\frac{2}{\pi\Gamma} M_p(\omega), \tag{5a}$$

$$\frac{\partial P_p(\omega)}{\partial\omega} = \frac{4}{\pi^2\Gamma}\left(\ln\left(\frac{\omega}{\omega_h}\right) + 1\right), \tag{5b}$$

and highlights that the modulus is a monotonous decreasing function of ω, with a limit value of

$$M_{P_h} = \exp\left(-\frac{2\omega_h}{\pi\Gamma}\right). \tag{6}$$

Additionally, the phase reaches a minimum value:

$$P_{P_m} = -\frac{4\omega_h}{e\pi^2\Gamma}, \tag{7}$$

Table 1. Frequency behaviour of the filter associated with anelastic propagation (modulus M_p and phase P_p).

ω	0		$\frac{\omega_h}{e}$		ω_h
$M_p(\omega)$	$+\infty$		$\searrow$		M_{P_h}
$P_p(\omega)$	0	$\searrow$	P_{P_m}	$\nearrow$	0

this occurs at the angular frequency ω_h/e where $e = \exp(1)$ (Table 1). This means that the anelastic propagation acts as a low-pass filter associated with a frequency-dependent phase rotation.

2.3. *Modulus and phase associated with the anelastic reflection contribution*

The seismic reflection that occurs at the anelastic interface is modelled by a step-like discontinuity between the upper anelastic layer M_1 where the seismic wave propagates, and a lower anelastic layer M_2 characterised by a density ρ_2, a reference velocity c_2 and a quality factor Q_2. Similar to M_1, M_2 is associated with a complex P-wave velocity $v_2^*(\omega) \simeq c_2(\frac{\omega}{\omega_h})^{\frac{1}{\pi Q_2}}[1 + \frac{i}{2Q_2}]$ and the reflection coefficient can thus be expressed as:

$$R^*(\omega) = \frac{\rho_2 c_2 \left(\frac{\omega}{\omega_h}\right)^{\frac{\eta}{\pi}} \left(1 + \frac{i}{2Q_2}\right) - \rho_1 c_1 \left(1 + \frac{i}{2Q_1}\right)}{\rho_2 c_2 \left(\frac{\omega}{\omega_h}\right)^{\frac{\eta}{\pi}} \left(1 + \frac{i}{2Q_2}\right) + \rho_1 c_1 \left(1 + \frac{i}{2Q_1}\right)}, \tag{8}$$

where we introduce the parameter

$$\eta = \frac{1}{Q_2} - \frac{1}{Q_1}, \tag{9}$$

that quantifies the anelastic contrast between the two layers.

To understand the filtering effects induced by the anelastic reflection coefficient on a normal incident plane wave, both the modulus and phase of R^* have to be expressed analytically. Such developments require expressing the anelastic reflection coefficient as the sum of its real and imagery parts. To do so, we use the decomposition $R^*(\omega) = R_E + R_A(\omega)$ established by Bourbié & Nur (1984) where

$$R_E = \frac{\rho_2 c_2 - \rho_1 c_1}{\rho_2 c_2 + \rho_1 c_1}, \tag{10}$$

represents the elastic impedance contrast that depends on the velocity and density parameters, and

$$R_A(\omega) = \frac{\eta}{2\pi} \ln\left(\frac{\omega}{\omega_h}\right) + i\frac{\eta}{4}, \tag{11}$$

represents the anelastic contribution that is complex and depends on η (equation (9)) and frequency. By introducing

Table 2. Frequency behaviour of the filter associated with anelastic reflection (modulus M_r and phase P_r).

	$\frac{R_E}{\eta} \leq 0$			$\frac{R_E}{\eta} > 0$				
ω	0		ω_h	0		ω_c		ω_h
$M_r(\omega)$	$+\infty$	$\searrow$	M_{r_h}	$+\infty$	$\searrow$	M_{r_m}	$\nearrow$	M_{r_h}
$P_r(\omega)$	π	$\searrow$	$P_{r_h} \geq \frac{\pi}{2}$	π	$\searrow$	$\frac{\pi}{2}$	$\searrow$	$P_{r_h} > 0$

the parameter:

$$D(\omega) = \frac{R_E}{\eta} + \frac{1}{2\pi} \ln\left(\frac{\omega}{\omega_h}\right), \tag{12}$$

this allows the reflection coefficient R^* to be expressed as:

$$R^*(\omega) = \eta D + i\frac{\eta}{4}, \tag{13}$$

which tends to R_E as η approaches 0 as expected for an elastic reflector. As a result, it is now straightforward to establish analytical formulations of the modulus $M_r = \sqrt{R_x^2 + R_y^2}$ and phase $P_r = \text{atan2}(R_x, R_y)$ of the reflection coefficient $R^* = R_x + iR_y$:

$$M_r(\omega) = \frac{|\eta|}{4}\sqrt{1 + 16D^2(\omega)}, \tag{14a}$$

$$P_r(\omega) = \text{atan2}(1, 4D(\omega)). \tag{14b}$$

These equations highlight that an anelastic reflection acts as a complex frequency filter that depends on both the anelastic contrast η and the ratio R_E/η between the elastic and anelastic contrasts.

The frequency response of the filter associated with the reflection on an anelastic interface is described by the partial derivatives of both the modulus and phase with respect to the angular frequency ω. We can show that

$$\frac{\partial M_r(\omega)}{\partial \omega} = \frac{\eta^2 D(\omega)}{M_r(\omega)\, 2\pi\omega}, \tag{15a}$$

$$\frac{\partial P_r(\omega)}{\partial \omega} = -\frac{\eta^2}{8\pi\omega M_r^2(\omega)}, \tag{15b}$$

where the modulus increases or decreases with ω depending on R_E/η and the phase is a monotonous decreasing function of ω. The asymptotic values of the partial derivatives when ω tends to 0 are $+\infty$ and 0, respectively, and

$$M_{r_h} = \frac{|\eta|}{4}\sqrt{1 + \left(4\frac{R_E}{\eta}\right)^2}, \tag{16a}$$

$$P_{r_h} = \text{atan2}\left(1, 4\frac{R_E}{\eta}\right), \tag{16b}$$

when ω tends to ω_h (Table 2). This means that the frequency filter associated with an anelastic reflection is asymmetric with respect to R_E/η whereby:

- if $R_E/\eta \leq 0$, the modulus and phase are monotonous decreasing functions of ω: the anelastic reflection acts as a low-pass filter, the phase response is nonlinear and ranges between an opposite and quadrature phase;
- if $R_E/\eta > 0$, the modulus is characterised by an extremum, i.e. $M_{r_m} = |\eta|/4$, that is located at the critical angular frequency

$$\omega_c = 2\pi\omega_h \exp\left(-2\pi\frac{R_E}{\eta}\right), \tag{17}$$

and is associated with a quadrature filter. At lower and higher frequencies, the modulus decreases and increases with ω, respectively, i.e. the anelastic reflection is not a simple low-pass filter and acts as a complex attenuating filter, ranging between an opposite and in-phase response.

3. Cumulative effects induced by anelastic propagation and reflection

3.1. *Modulus and phase associated with the anelastic propagation contribution*

The frequency filter that takes into account both a seismic propagation in an upper anelastic layer and a reflection by an anelastic interface is the cumulative frequency filter. It is defined by the following modulus M and phase P:

$$M(\omega) = M_p(\omega) M_r(\omega), \tag{18a}$$

$$P(\omega) = P_p(\omega) + P_r(\omega). \tag{18b}$$

The global filter is characterised by a frequency-dependent phase rotation because $P_p(\omega)$ has a minimum located at the angular frequency ω_h/e and $P_r(\omega)$ is a monotonous decreasing function of ω: additive contributions of the anelastic propagation and reflection effects occur when $\omega < \omega_h/e$ and the opposite occurs when $\omega > \omega_h/e$. The frequency response of the phase can thus be assessed analytically based on equations (5b) and (15b).

Table 3. Frequency behaviour of the filter associated with anelastic reflection (modulus M and phase P).

	$\frac{R_E}{\eta} \leq 0$			$\frac{R_E}{\eta} > 0$						
ω	0		ω_h	0		$\omega_{c'}$		$\omega_{c''}$		ω_h
$M(\omega)$	$+\infty$	$\searrow$	$M_{p_h}M_{r_h}$	$+\infty$	$\searrow$	min	If $\eta < \eta_c(\tau)$ $\nearrow$ If $\eta > \eta_c(\tau)$ $\searrow$	max	$\searrow$	$M_{p_h}M_{r_h}$

Similarly, the cumulative filter is characterised by a frequency-dependent modulus but the frequency response defined as

$$\frac{\partial M(\omega)}{\partial \omega} = M_p(\omega)\frac{\partial M_r(\omega)}{\partial \omega} + M_r(\omega)\frac{\partial M_p(\omega)}{\partial \omega} \qquad (19)$$

does provide straightforward analytical solution. The frequency response depends on R_E/η and its behaviour can be summarised as follows (Table 3):

- if $R_E/\eta \leq 0$, $M_p$and M_r are both monotonous decreasing functions of the angular frequency ω, i.e. the cumulative filter is equivalent to a low-pass-filter with additive contributions of the anelastic propagation and reflection effects;
- if $R_E/\eta > 0$, $M_p$is still a monotonous decreasing function of ω but M_r is characterised by a minimum value M_{r_m} located at the critical frequency ω_c. The number of roots for equation (19) depends on the physical parameters. Consequently, a numerical solution is required if further quantitative analysis is to be performed, allowing the descriptions reported in Table 3.

A numerical application with realistic values of the physical parameters is now performed to quantitatively assess the contributions of both the anelastic propagation and reflection in the frequency domain for different elastic R_E and anelastic η contrasts.

3.2. *Numerical investigation*

The aim of the numerical evaluation, performed over a large range of physical parameters, is to quantify the frequency filtering effects that include both the anelastic propagation and reflection contributions.

For the anelastic propagation contribution, we consider $Q_1 = 100$ and $\tau = 100$ ms, which corresponds to $\Gamma = 1273$ Hz. The attenuation $(20 \log M_p)$ and the phase P_p are represented as functions of the normalised frequency $f_n = \omega/\omega_h$ in the frequency bandwidth 0–150 Hz (figures 2a and 3a). For the anelastic reflection contribution, which depends on R_E/η, we determine the attenuation $(20 \log M_r)$ and phase P_r for three elastic reflection coefficients $R_E = -0.025$, 0 and 0.025 and η ranging from 0 to 0.2 with $Q_1 = 100$ (figures 2b1–3 and 3b1–3). Note that changing Q_1 to a lower value while keeping η constant only affects the propagation contribution, both in amplitude and phase according to equations (4a) and (4b), but does not affect the reflection contribution. The case $R_E = 0$ corresponds to a pure anelastic reflection induced by the constant-Q contrast only: for instance, when $\eta \simeq 0.1$, the attenuation is about 30 dB. Note that this is similar to the attenuation of 32 dB associated with the pure elastic case $\eta = 0$ with $R_E = \pm 0.025$. The cumulative effects of both the anelastic propagation and reflection are solved numerically to display the attenuation $(20 \log M)$ and P (figures 2c1–3 and 3c1–3) of the cumulative filter.

As expected by the previous analytical developments, (i) the filter associated with the anelastic propagation is equivalent to a low-pass filter with a frequency-dependent phase rotation, (ii) the filter associated with the anelastic reflection is equivalent to a low-pass filter with a frequency-dependent phase rotation when $R_E \leq 0$ and characterised by a critical frequency when $R_E > 0$, and (iii) the cumulative filter is equivalent to a low-pass filter with a frequency-dependent phase rotation when $R_E \leq 0$. The numerical investigation highlights three main effects induced by the interaction of the propagation and reflection contributions when $R_E > 0$: (i) it removes the critical frequency ω_c when $\eta > \eta_c$ where η_c is a critical value of η above which the modulus of the cumulative filter becomes a monotonous decreasing function of the frequency ($\eta_c \simeq 0.11$ in the present case), (ii) modifies ω_c into $\omega_{c'}$ when $\eta_{c'} < \eta$ (figure 2c3, solid line) and (iii) induces a second critical frequency $\omega_{c''} > \omega_{c'}$ when $\eta_{c''} < \eta_{c'}$ (figure 2c3, dot-dashed line). We show that these critical curves $(\omega_{c'}, \eta_{c'})$ and $(\omega_{c''}, \eta_{c''})$ depend on τ (figure 4) and as a result, the cumulative filter modulus can be characterised by zero, one (case $\tau \to 0$) or two critical frequencies, i.e. the filter can be a low-pass, a band-pass or a high-pass filter depending on η and τ when $R_E > 0$ (figure 2c3).

This result means that for some particular cases, high frequencies of a seismic signal may be less attenuated than low frequencies when anelastic reflection is taken into account: this unexpected behaviour is controlled by the sign of the parameter D described in equation (12). These quantitative analyses are of first importance to better understand

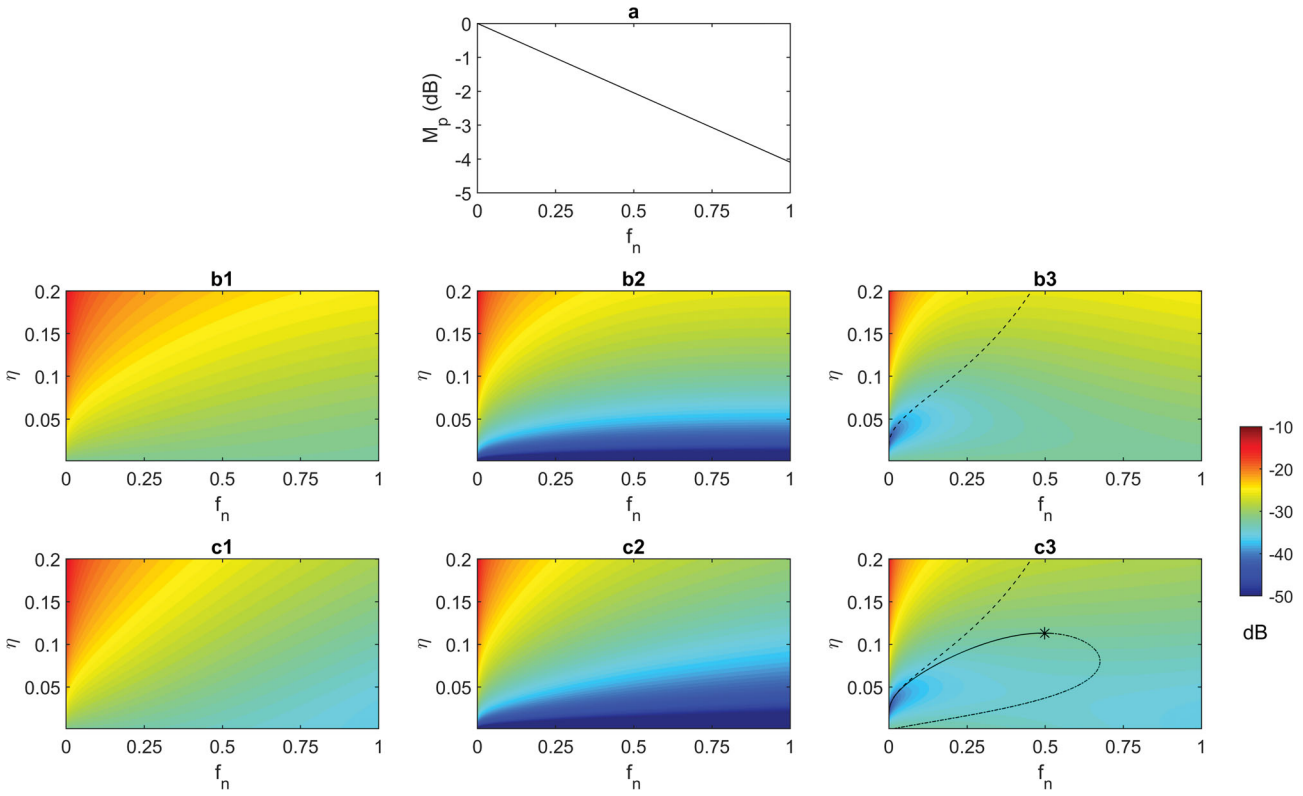

Figure 2. (a) Modulus spectrum associated with the anelastic propagation contribution (normalised frequency $f_n = \omega/\omega_h$). Modulus spectra associated with the anelastic reflection contribution for a negative (b1), null (b2) and positive (b3) R_E. (c1, c2 and c3) Modulus spectra associated with the cumulative effects of both the anelastic propagation and reflection for the three R_E values. The dashed curves follow the critical frequency ω_c (equation (17)) associated with the anelastic reflection contribution. The critical value η_c is indicated with a black star. The solid and dot-dashed curves follow the minimum and maximum amplitude values, respectively (numerical solution).

the effects of both the anelastic propagation and reflection phenomena on seismic signals.

4. Anelastic effects induced on a seismic source

4.1. *Peak-frequency attributes associated with a Ricker source wavelet*

In this section, we investigate the effect of the cumulative filter associated with both anelastic propagation and reflection on a seismic signal by approximating the seismic incoming signal $\psi(t)$ with a Ricker wavelet. This wavelet, widely used to model a seismic source in geophysical prospecting (Wang 2015a), is a zero-phase signal expressed in the frequency domain by Wang (2015a):

$$\Psi(\omega) = \frac{2\omega^2}{\sqrt{\pi}\omega_p^3} \exp\left(-\frac{\omega^2}{\omega_p^2}\right), \qquad (20)$$

where $\omega_p = 2\pi F_P$, with F_P the peak frequency defined as the frequency associated with the maximum amplitude of $\Psi(\omega)$. The peak frequency can be analytically described in the framework of propagation effects of anelasticity (Zhang & Ulrych 2002; Tary *et al.* 2017) for evaluating the Q factor. The present work extends these developments by including the reflection contribution. This cannot be undertaken when considering the central frequency (Wang 2015a), which can only be solved numerically. The use of the peak frequency constitutes a quantitative support for seismic analysis to better understand the physical phenomena discussed in the present study.

The signal $\psi'(t)$ measured after a seismic propagation of the Ricker wavelet through the anelastic upper layer and a reflection at the anelastic interface is defined by the modulus $M'(\omega) = \Psi(\omega)M(\omega)$ and the phase $P(\omega)$. The peak frequency F_P is changed into the peak-frequency attribute F'_p defined as the solution $\omega'_p = 2\pi F'_p$ of $\frac{\partial M'}{\partial \omega} = 0$ (Ker *et al.* 2012; Wang 2015b). In the following, the amplitude A'_p and phase ζ'_p of $\psi'(t)$ at F'_p are the peak-frequency attributes used as complementary attributes in the present quantitative analysis of the wavelet distortion induced by the anelastic processes. The shape changing of the seismic wavelet, during propagation in the upper anelastic layer and reflection at the interface with the lower layer, is implicitly considered in the present analytical solution. The peak-frequency attribute is influenced

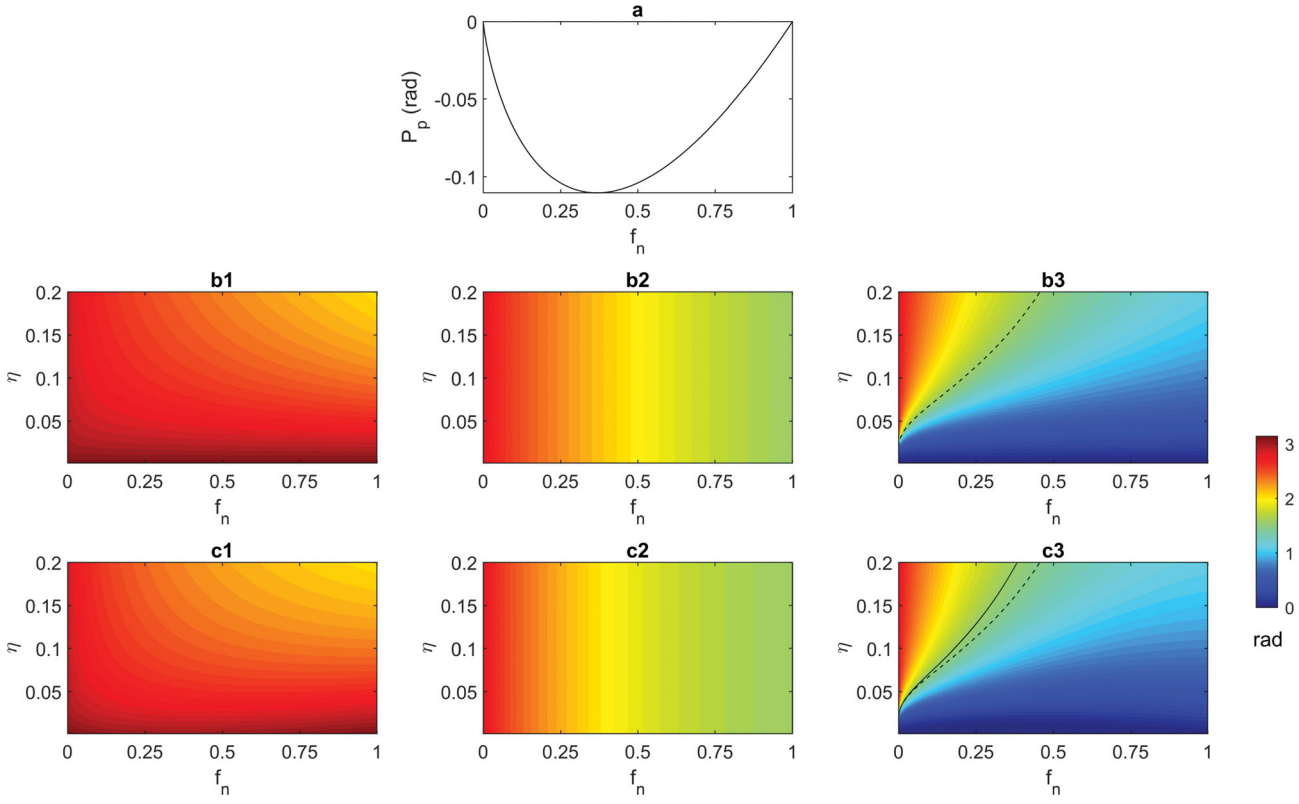

Figure 3. (a) Phase spectrum associated with the anelastic propagation contribution (normalised frequency $f_n = \omega/\omega_h$). Phase spectra associated with the anelastic reflection contribution for a negative (b1), null (b2) and positive (b3) R_E. (c1, c2 and c3) Phase spectra associated with the cumulative effects of both the anelastic propagation and reflection for the three R_E values. The dashed curves follow the critical frequency ω_c (equation (17)) associated with the quadrature filter induced by the anelastic reflection contribution. The solid curve follows the quadrature filter induced by both the anelastic propagation and reflection (numerical solution).

by the increasing asymmetry of the amplitude spectrum of the reflected wavelet generated by both propagation and reflection filters. In addition, the phase attribute ζ_p' is influenced by the effect of the wavelet shape changing induced by the cumulative filter on the phase spectrum of the reflected wavelet.

Based on the analytical developments presented in the previous section, we show that the peak-frequency attribute of the reflected signal associated with a Ricker seismic source wavelet is given by

$$F_p' = F_p\left(\sqrt{\frac{F_p^2}{\Gamma^2} + 1 + B(\omega)} - \frac{F_p}{\Gamma}\right), \tag{21}$$

where the parameter

$$B(\omega) = \frac{1}{\pi}\frac{4D(\omega)}{1 + 16D^2(\omega)}, \tag{22}$$

quantifies the contribution of the anelastic reflection coefficient. We can show that B ranges between $\pm 1/2\pi$. Equation (21) can be solved numerically but to develop an analytical expression, we consider that $B(\omega)$ is dominated by the contribution of the peak-frequency attribute F_{p_p} related to the anelastic propagation, i.e. $B(\omega) \simeq B(\omega_{p_p})$ where $\omega_{p_p} = 2\pi F_{P_p}$ is the solution of $\frac{\partial(\Psi M_p)}{\partial\omega} = 0$. We show that

$$F_{p_p} = F_p\left(\sqrt{\frac{F_p^2}{\Gamma^2} + 1} - \frac{F_p}{\Gamma}\right) \leq F_p. \tag{23}$$

The present work focuses on the impact of the anelastic contrast η on the peak-frequency modification and thus requires analysing $\frac{\partial F_p'}{\partial\eta}$ by fixing Q_1 in the upper layer, i.e. we investigate the behaviour of F_p' with changes of Q_2 only. The limit $F_{p\infty}'$ when Q_2 tends to 0, which corresponds to η tending to infinity, is outside the validity range of the present work but a rough estimate is given in the Appendix. When Q_2 tends to Q_1, which corresponds to η tending to 0, we show that the limit is $F_{p0}' = F_{p_p}$. This analysis is limited to a Q_2 value between 0 and Q_1 as results associated with negative η values are identical to those obtained by changing the sign of R_E (i.e. the consequence of the dependency on the sign of R_E/η as described in Section 3). We demonstrate that the

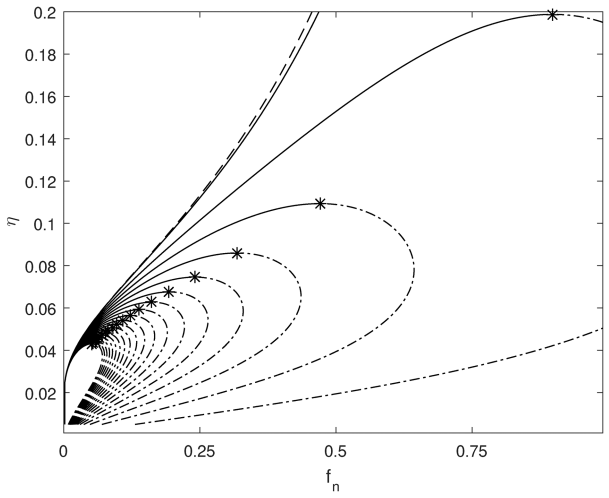

Figure 4. Representation of η_c (black star), $\omega_{c'}$ (solid curve) and $\omega_{c''}$ (dot-dashed curve) for different travel times τ ranging between 5 ms and 1 s in steps of 50 ms (numerical solution). When τ tends to 0, the curve $\omega_{c'}$ tends to the critical frequency ω_c (equation (17)) associated with the anelastic reflection contribution (dashed curve).

partial derivative of F'_p in relation to Q_2 is expressed as

$$\frac{\partial F'_p}{\partial Q_2} = \frac{2}{\pi}\frac{Q_1^2}{(Q_2-Q_1)^2}\frac{F_p}{\left(\frac{F'_p}{F_p}+\frac{F_p}{\Gamma}\right)}R_E\frac{1-16D^2(\omega_{p_p})}{1+16D^2(\omega_{p_p})}. \tag{24}$$

When $R_E \leq 0$, the peak frequency is monotonous and $F'_p \leq F_{p_p}$, with an increasing trend with Q_2 meaning that F'_p decreases with η. For the case $R_E = 0$, F'_p is a constant similar to $F'_{p\infty}$.

When $R_E > 0$, F'_p is not monotonous but characterised by two extrema located at two particular Q_2 values. Only one corresponds to $Q_2 < Q_1$ and is expressed by

$$F'_{p_e} = F_p\left(\sqrt{\frac{F_p^2}{\Gamma^2}+1+\frac{1}{2\pi}}-\frac{F_p}{\Gamma}\right) > F_p. \tag{25}$$

It does not depend on R_E and is located at

$$\eta_e = R_E\left(\frac{1}{4}-\frac{1}{2\pi}\ln\left(\frac{F_{p_p}}{F_h}\right)\right)^{-1}. \tag{26}$$

When $0 \leq \eta \leq -\frac{2\pi R_E}{\ln(F_{p_p}/F_h)}$, F'_p increases from F_{p_p} when $\eta = 0$ up to F'_{p_e} and then decreases to F_{p_p}. Additionally, we note that

$$F'_p \geq F_p \text{ when } \begin{cases} Q_1 \geq \pi^2\tau F_p \\ \eta_- \geq \eta \geq \eta_+ \end{cases}, \tag{27}$$

where $\eta_\pm = R_E\left(\frac{Q_1 \pm \sqrt{Q_1^2-(\pi^2\tau F_p)^2}}{4\pi^2\tau F_p}-\frac{1}{2\pi}\ln\left(\frac{F_{p_p}}{F_h}\right)\right)^{-1}$. The existence of the unexpected phenomenon $F'_p \geq F_p$ associated with a step-like interface is based on the condition $\tau < \frac{Q_1}{\pi^2 F_p}$, which deals with the anelastic propagation in the upper layer only.

For the peak-frequency attributes A'_p and ζ'_p, we develop analytical expressions in relation to Q_2, i.e. with η when Q_1 is fixed based on approximations detailed in the Appendix and used here. The analysis predicts that A'_p is a monotonous increasing function of η if $R_E \leq 0$, but is characterised by an extremum if $R_E > 0$, located at $R_E\left(\frac{-\pi}{8\ln\left(\frac{F_{p_p}}{F_h}\right)}-\frac{1}{2\pi}\ln\left(\frac{F_{p_p}}{F_h}\right)\right)^{-1}$ which differs from η_e. The analysis also predicts that ζ'_p decreases or increases monotonically with η from $\zeta'_{p\infty}$ to ζ_{p_p} (see Appendix) if $R_E < 0$ or $R_E > 0$, respectively, and is similar to $\zeta'_{p\infty}$ if $R_E = 0$.

4.2. *Numerical applications to quantify the anelastic Ricker wavelet distortions*

The analytical expressions developed previously allow general considerations of the Ricker wavelet distortion induced by the anelastic processes. To illustrate the results, we consider the following parameters: the peak frequency of the Ricker source wavelet is $F_P = 50$ Hz, $R_E = -0.025$, 0 and 0.025, $Q_1 = 100$ and $\tau = 100$ ms. We determine the reflected seismic signal as a function of η in the range $[0; 0.2]$, which corresponds to a Q_2 range of $[5; 100]$, both in the time and frequency domains (figures 5 and 6). Note that because the Ricker frequency content is theoretically unlimited, the reference upper frequency F_h has to be defined in order to be able to perform the analyses. In practice, this may be controlled by a threshold on the signal-to-noise ratio: an arbitrary threshold of 0.3 % corresponds to $F_h = 150$ Hz.

When η tends to 0, the waveform associated with $R_E < 0$ (figure 5a1) is in the opposite phase with the one associated with $R_E > 0$ (figure 5a3), which is similar to the shape of the Ricker source wavelet, and for $R_E = 0$ (figure 5a2), the amplitude of the waveform tends to 0. When η increases to 0.2, reflected waveforms for the three cases look similar but strongly differ for intermediate η values. This behaviour is quantified by the associated modulus and phase spectra displayed with respect to η (figure 6), in accordance with the analytical results developed in the previous section. In particular, the peak-frequency attribute F'_p (figure 6, blue curves) decreases monotonously with η when $R_E < 0$, is constant when $R_E = 0$ and is characterised by an extremum when $R_E > 0$ where F'_p can be larger than F_p (figure 6, dashed-black lines). It is interesting to note that (i) measuring $F'_p > F_p$ means that both $R_E > 0$ and η are between $\eta_{c'}$ and $\eta_{c''}$ (figure 7a1, dashed-green lines), with the condition

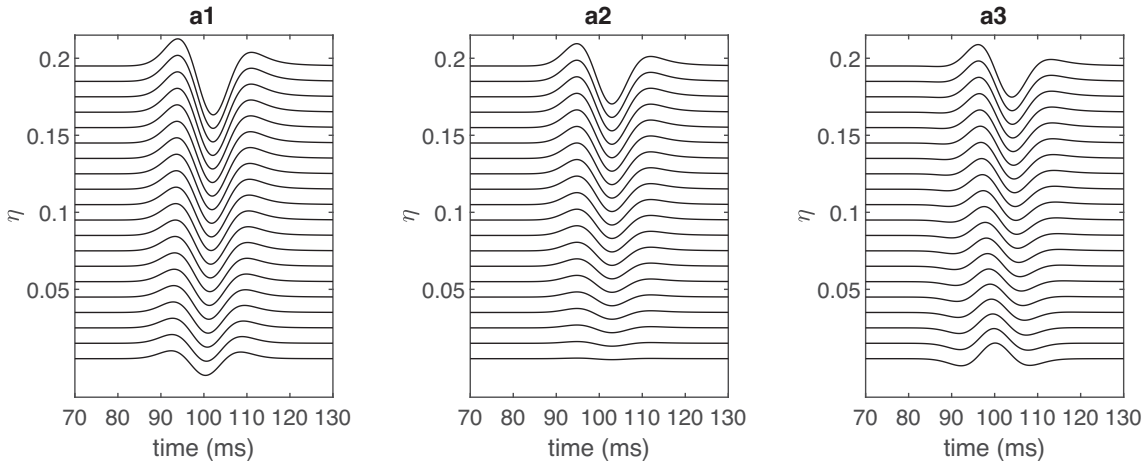

Figure 5. Synthetic seismic signals associated with a 50 Hz Ricker source wavelet after a propagation in an anelastic layer and a reflection by an anelastic reflector according to the equivalent cumulative filter (figures 2 and 3) for a negative (a1), null (a2) and positive (a3) elastic impedance contrast R_E.

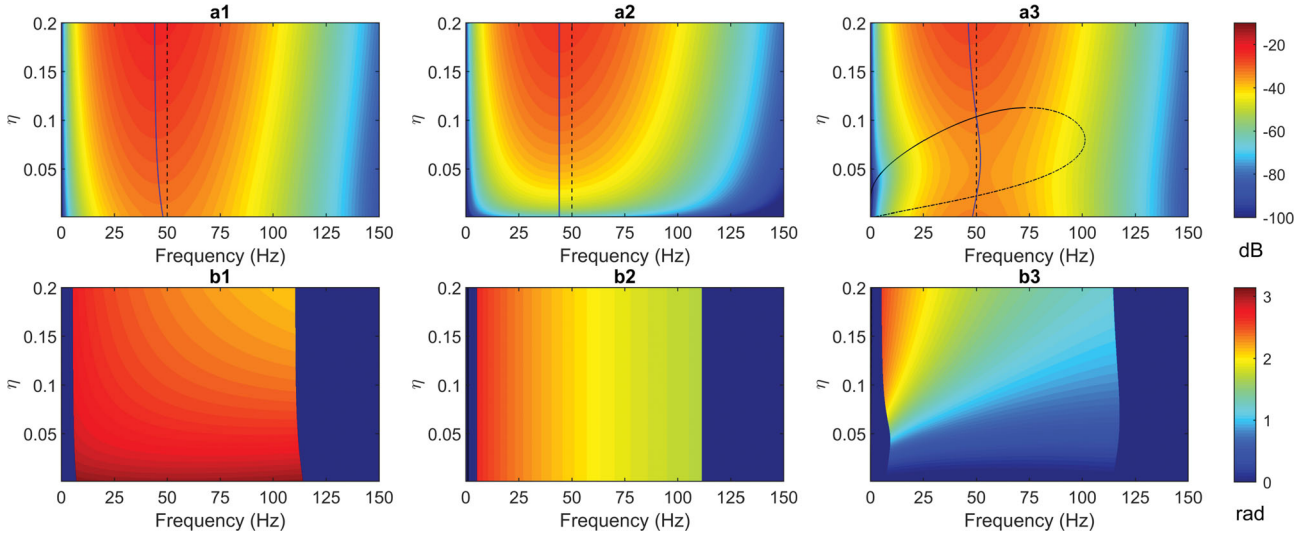

Figure 6. (a1–3) Modulus spectra of the signals displayed in figure 5 associated with a Ricker source wavelet of peak frequency $F_p = 50$ Hz (dashed line) modified into the attribute F'_p (equation (21)) by the anelastic cumulative filter for a negative (left), null (middle) and positive (right) R_E. The solid and dot-dashed-black curves follow the minimum and maximum amplitudes of the cumulative filter, respectively (numerical solution). (b1–3) Phase spectra of the signals displayed in figure 5: a mask defined on the modulus spectrum by a threshold of −24 dB has been applied to focus on the main representative frequency content.

$\tau < \frac{Q_1}{\pi^2 F_p}$ being satisfied, and (ii) whatever the value of R_E, the peak frequency measured on the reflected signal is limited to the range [44; 52 Hz] (figure 7a1–3). This highlights relative changes of the peak-frequency attribute limited to [−8; 4%]. Importantly, η can be assessed from F'_p when $R_E < 0$ but uncertainties increase when F'_p tends to 44 Hz.

The two peak-frequency attributes associated with F'_p are also used to quantify the Ricker wavelet distortions. First, the amplitude A'_p (figure 7b1–3, blue curves) increases with η when $R_E \leq 0$, and is characterised by an extremum when $R_E > 0$. Amplitude variations are about 10 dB when $R_E \neq 0$ and about to 20 dB when $R_E = 0$. Second, the phase ζ'_p (figure 7c1–3, blue curves) strongly depends on both η and the sign of R_E: it highlights a phase rotation that decreases with η in a limited range [2.5; 3 rad] when $R_E < 0$, is constant to about 2 rad if $R_E = 0$, and varies from in-phase to opposite phase when $R_E > 0$ in the range [−0.1; 1.7 rad]. As a result, the phase of the cumulative filter significantly contributes to the variations in the reflected wavelet observed in the time domain (figure 5).

It is important to remember that the phase spectrum of the reflected signal associated with a zero-phase Ricker source wavelet is given by the phase of the cumulative filter. In order to focus on the phase rotation around the main frequency content of the reflected signal, we apply a mask

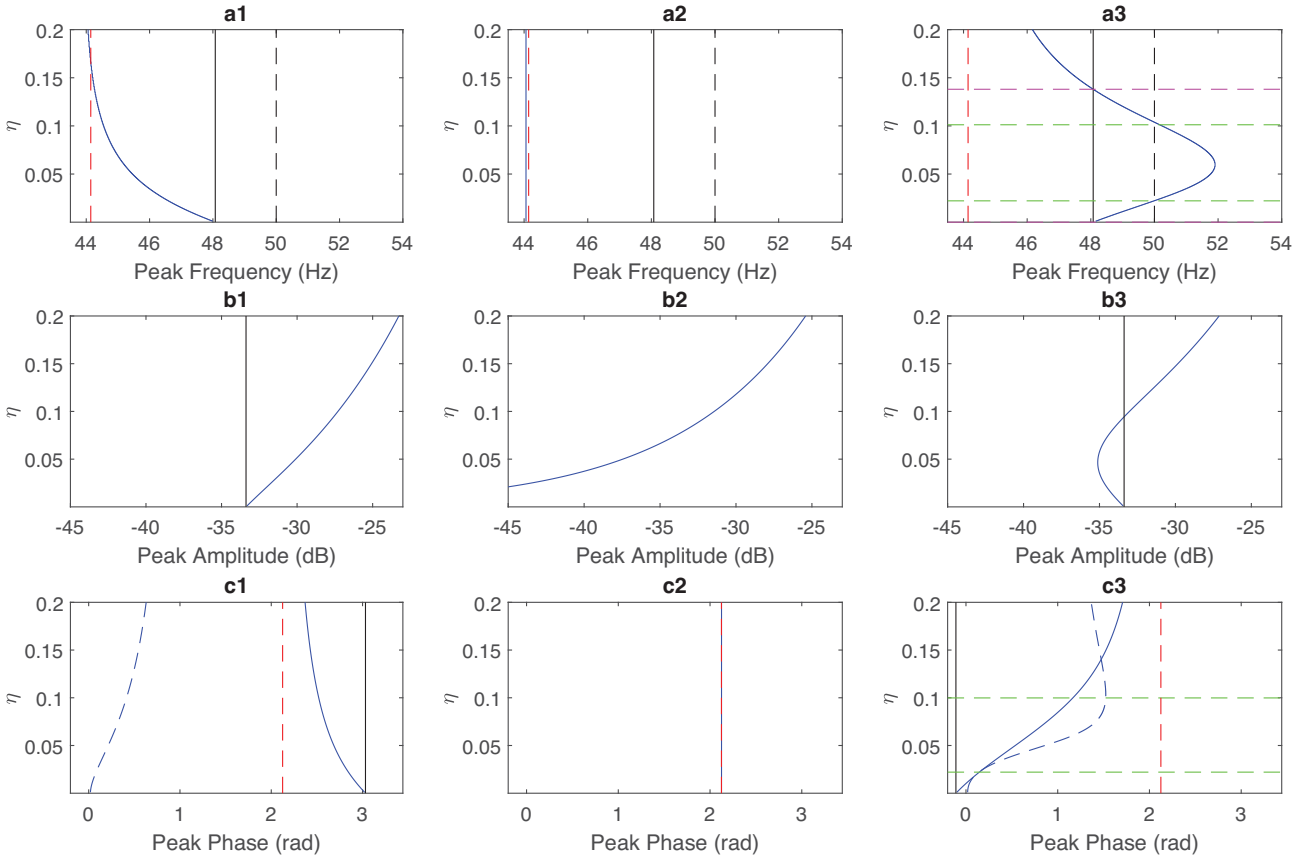

Figure 7. Seismic peak-frequency attributes (blue curves) associated with a Ricker source wavelet of peak frequency F_p= 50 Hz (dashed-black line) modified by the cumulative filter for a negative (left), null (middle) and positive (right) R_E. (a1–3) The peak-frequency attribute F'_p (equation (21), blue curve) ranges between $F_{p_p} \simeq 48$ Hz (equation (23), black line) and $F'_{p\infty}$ (equation (32a), black line). Dashed magenta and green lines define the interval where $F'_p \geq F'_{p_p}$ and $F'_p \geq F_p$ (equation (27)), respectively. (b1–3) The amplitude attribute A'_p (equation (31b), blue curve) associated withF'_p: the black line represents the amplitude of the modulus spectrum at the frequency F_{p_p}. (c1–3) The phase attribute ζ'_p (equation (31c), blue curve) associated with F'_p: the black line represents the phase at the frequency F_{p_p} and the dashed blue curve represents the phase range (see figures 6b1–3) with strong variations located in the range $F'_p \geq F_p$ (dashed-green lines).

defined by an amplitude threshold, fixed here to −24 dB on the modulus (figure 6b1–3): the difference between the minimum and maximum values of the phase monotonously increase with η when $R_E < 0$ but is characterised by an extremum when $R_E > 0$ where most of the phase variations occurs between $\eta_{c'}$ and $\eta_{c''}$ (figure 7c1 and 3, dashed lines).

4.3. *Discussions on the peak-frequency attribute: pitfalls and insights*

As quantified by the numerical example described above, the second order contribution of the anelastic propagation can be neglected in most realistic cases, *i.e.* $\frac{F_p^2}{\Gamma^2} << 1$. This allows us to neglect the case where a seismic wave vanishes in the upper layer and considering $F_{p_p} \simeq F_p(1 - \frac{F_p}{\Gamma})$ and $F'_p \simeq F_p(\sqrt{1+B} - \frac{F_p}{\Gamma})$ for sake of simplicity. Recall that $\Gamma = 4Q_1/\pi\tau$.

The peak-frequency attribute F'_p is commonly used to assess the quality factor Q_1 of the upper layer. The approach is based on the assumption that $\eta = 0$, i.e. the anelastic contribution of the reflection is negligible. In this case, a first approximation consists in $F'_p \simeq F_{p_p}$ which allows relating Q_1 and F'_p according to $Q_1 \simeq \frac{\pi\tau F_p}{4(1-F'_p/F_p)}$. But this relation induces errors when anelastic reflection is not negligible. Based on the present study, we are able to quantify the modification of F'_p when η is taken into account, and as a result, the impact on the Q_1 assessment. The modification of F'_p with η relatively to F_{p_p} is quantified by $\Delta F = (F'_p - F_{p_p})/F_{p_p}$, which highlights a dependency with both η, R_E and τ (figure 8a1 and 2), and induces a relative modification of Q_1 quantified by ΔQ_1 (figure 8b1 and 2). When $R_E < 0$, ΔF is negative and its amplitude increases with both η and τ by up to 10% (figure 8a1): assessing Q_1 from F'_p, whose relationship is nonlinear, results in an underestimation of 20% that increases to 75% at large

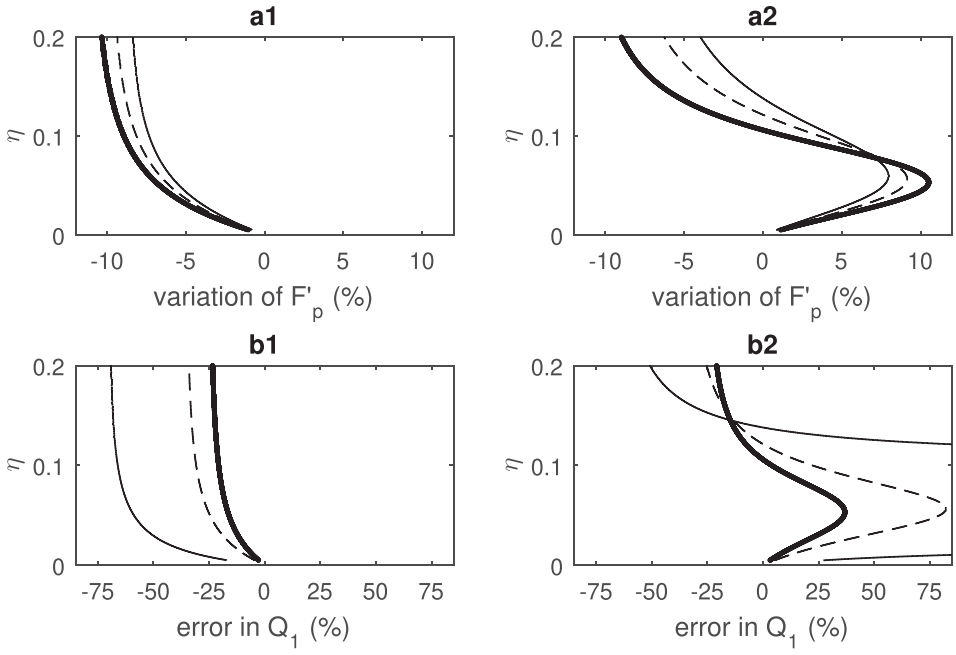

Figure 8. (a1–2) Modifications ΔF of the peak-frequency attributeF'_p, relative to F_{p_p} associated with a negligible anelastic contrast $\eta = 0$, as a function of η for a negative (left) and positive (right) elastic contrast R_E. Results for different travel times τ are displayed (0.1, 0.5 and 1 s as solid, dashed and bold curves, respectively). (b1–2) Error in Q_1 estimate based on the peak-frequency attribute F'_p as a function of η.

travel times (figure 8b1). When $R_E > 0$, ΔF is more complex (figure 8a2) and mainly induces an overestimation of Q_1 (figure 8b2): regardless of the value of τ, the minimum error occurs when η reaches the value $-\frac{2\pi R_E}{\ln(F_{p_p}/F_h)}$ (see section 4.1).

To go beyond these particular numerical examples, it is interesting to observe the approximated linear dependency of ΔF with η when η is low. We can demonstrate that at large R_E/η values, i.e. roughly larger than unity, $F'_p \simeq F_p(1 + \frac{\eta}{8\pi R_E} - \frac{F_p}{\Gamma})$ and the modification of the peak-frequency attribute can be approximated as

$$\Delta F \simeq \eta \left[8\pi R_E \left(1 - \frac{F_p}{\Gamma} \right) \right]^{-1}. \tag{28}$$

This result analytically predicts a significant modification of F'_p even at low η values. In addition, it also demonstrates a weak dependency with Q_1 and τ, quantified by F_p/Γ, implying a low contribution of the effects of the anelastic propagation in the relative modification ΔF of the peak-frequency attribute. Finally, we show that the error in assessing Q_1 when η is low can be expressed by the approximation

$$\Delta Q_1 \simeq \left[\frac{8\pi R_E}{\eta} \frac{F_p}{\Gamma} - 1 \right]^{-1} = \left[2\pi^2 F_p \tau \frac{R_E}{\frac{Q_1}{Q_2} - 1} - 1 \right]^{-1}, \tag{29}$$

which is nonlinear in η and depends on Q_1/Q_2. Note that an underestimation of Q_1 is expected if $R_E < 0$ and that according to equation (29), the error in Q_1 increases when F_P decreases. For example, the error is almost doubled when F_P decreases from 50 to 30 Hz.

5. Conclusions

In the present work, we have quantified the effects induced by both anelastic propagation and reflection by performing analytical developments of the equivalent cumulative filter defined in the framework of Kjartansson's model for a step-like reflector. In particular, the cumulative filter is characterised by an asymmetrical frequency behaviour that depends on the ratio R_E/η between the elastic reflection coefficient of the reflector and the anelastic contrast between the upper and lower layers. In most cases, the cumulative filter acts as a low-pass filter in agreement with the classical understanding that higher seismic frequencies are more attenuated than low frequencies. The band- or high-pass behaviour occurs only for a limited range of source peak frequency, η parameter and travel time τ, and when the signs of η and R_E are the same: this unexpected behaviour constitutes a key result.

In order to quantify the impact of the cumulative filter on an incoming seismic wave at normal incidence, we have developed analytical expressions for a Ricker source wavelet defined by a peak frequency. Because of the anelasic reflection, the reflected seismic signal is modified: its peak frequency and related amplitude and phase are used as attributes to quantify the distortions of the incoming source signal. We

show that the peak frequency depends on the sign of R_E/η. The effect of a negative ratio is to amplify both the shift of the peak frequency and the phase rotation induced by the anelastic propagation contribution. With a positive ratio, the effect is to decrease the shift of the peak frequency. We also highlight that the peak frequency can be larger than the source peak frequency, an unexpected phenomenon for a step-like interface controlled by the two critical frequencies of the cumulative filter when $\tau < \frac{Q_1}{\pi^2 F_p}$. The consequence of the cumulative filter is to introduce fluctuations in the peak frequency that cannot be explained by considering anelastic propagation alone as is commonly assumed when estimating the Q factor from the peak frequency. For a 50 Hz Ricker source wavelet, the modification of the peak-frequency attribute relative to the propagation contribution can be as high as 10%, with a strong impact when assessing the quality factor of the layer above the anelastic reflector. Errors arise as soon as η is not negligible and follow a nonlinear relationship with η.

The accuracy of the Q value estimation based on the peak frequency of a seismic wave reflected by an anelastic reflector depends on many physical parameters, as analytically demonstrated in this work that considered a Ricker wavelet. Consequently, estimating the quality factor of the upper layer from this seismic attribute alone is not a well-constraint inversion problem. A suggestion would be to consider further quantification in taking advantage of the full set of peak-frequency attributes introduced in this study in a simultaneous inversion scheme to assess both the elastic reflection coefficient and the constant-Q parameters defining the anelastic reflector.

Acknowledgements

We thank two anonymous reviewers for their comments that help us to improve this paper. We sincerely thank Shane Murphy for the revision of the English language.

Conflict of interest statement. None declared.

Appendix

Seismic attributes associated with the propagation in an anelastic layer with $\Gamma = 4Q_1/\pi\tau$

$$F_{p_p} = F_p\left(\sqrt{\frac{F_p^2}{\Gamma^2}+1}-\frac{F_p}{\Gamma}\right) = \omega_{p_p}/2\pi < F_p, \tag{30a}$$

$$A_{p_p} = \left|R_E\right|\Psi(\omega_{p_p})\exp\left(-\frac{4F_{p_p}}{\Gamma}\right), \tag{30b}$$

$$\zeta_{p_p} = \begin{cases} \frac{8}{\pi}\frac{F_{p_p}}{\Gamma}\ln\left(\frac{F_{p_p}}{F_h}\right)+\pi & : \text{when } R_E \le 0 \\ \frac{8}{\pi}\frac{F_{p_p}}{\Gamma}\ln\left(\frac{F_{p_p}}{F_h}\right) & : \text{when } R_E > 0 \end{cases}. \tag{30c}$$

Seismic attributes associated with both an anelastic propagation and an anelastic reflection

$$F'_p = F_p\left(\sqrt{\frac{F_p^2}{\Gamma^2}+1+B(\omega_{p_p})}-\frac{F_p}{\Gamma}\right) = \omega'_p/2\pi, \tag{31a}$$

$$A'_p = \frac{1}{4}\Psi(\omega'_p)\exp\left(-\frac{4F'_p}{\Gamma}\right)\sqrt{\eta^2\left(1+16D^2(\omega_{p_p})\right)}, \tag{31b}$$

$$\zeta'_p \simeq \frac{8}{\pi}\frac{F'_p}{\Gamma}\ln\left(\frac{F'_p}{F_h}\right)+\operatorname{atan2}\left(1,4D(\omega_{p_p})\right). \tag{31c}$$

Asymptotic limits when η *tends to infinity*

The limit when η is large is equivalent to Q_2 tends toward 0 for Q_1 fixed in the upper layer. This is outside the validity range of the approximations used in the present study but as a first estimate, the asymptotic limits of the peak frequency and phase attributes can be expressed by:

$$F'_{p\infty} = F_p\left(\sqrt{\frac{F_p^2}{\Gamma^2}+1+\frac{2\ln\left(F_{p_p}/F_h\right)}{\left(2\ln\left(F_{p_p}/F_h\right)\right)^2+\pi^2}}-\frac{F_p}{\Gamma}\right) \tag{32a}$$

$$\zeta'_{p\infty} \simeq \frac{8}{\pi}\frac{F'_{p\infty}}{\Gamma}\ln\left(\frac{F'_{p\infty}}{F_h}\right)+\operatorname{atan2}\left(1,\frac{2}{\pi}\ln\left(\frac{F'_{p\infty}}{F_h}\right)\right). \tag{32b}$$

Behaviour of F'_p *with* Q_2

$$\frac{\partial F'_p}{\partial Q_2} = \frac{2}{\pi}\frac{Q_1^2}{\left(Q_2-Q_1\right)^2}R_E\kappa, \tag{33a}$$

$$\kappa = \frac{F_p}{\left(\frac{F'_p}{F_p}+\frac{F_p}{\Gamma}\right)}\frac{1-16D^2(\omega_{p_p})}{1+16D^2(\omega_{p_p})}. \tag{33b}$$

Behaviour of A'_p with Q_2:

$$\frac{\partial A'_p}{\partial Q_2} = \frac{A'_p Q_1^2}{(Q_1 - Q_2)^2} R_E \left[\left(1 + \frac{\kappa}{\pi^2 F'_p} \right) \times \left(\frac{16D\left(\omega'_p\right)}{1 + 16D^2\left(\omega'_p\right)} - \frac{16D\left(\omega_{p_p}\right)}{1 + 16D^2\left(\omega_{p_p}\right)} \right) + \frac{16D\left(\omega_{p_p}\right)}{1 + 16D^2\left(\omega_{p_p}\right)} - \frac{\eta}{R_E} \right]. \quad (34)$$

The behaviour of the parameter D with the frequency is inversely proportional to the frequency and with $F'_p >> 1$ similar in magnitude to F_{p_p}, a first approximation consists in replacing $D(\omega'_p)$ by $D(\omega_{p_p})$, which gives

$$\frac{\partial A'_p}{\partial Q_2} \simeq \frac{A'_p Q_1^2}{(Q_1 - Q_2)^2} R_E \left[+ \frac{16D(\omega_{p_p})}{1 + 16D^2(\omega_{p_p})} - \frac{\eta}{R_E} \right]. \quad (35)$$

A minimum amplitude is located at the quality factor $\frac{1}{Q_1} - R_E\left(\frac{\pi}{8\ln\left(\frac{F_{p_p}}{F_h}\right)} + \frac{1}{2\pi}\ln\left(\frac{F_{p_p}}{F_h}\right)\right)^{-1}$ if $R_E > 0$.

Behaviour of ζ'_p with Q_2

$$\frac{\partial \zeta'_p}{\partial Q_2} = \frac{-4Q_1^2}{(Q_2 - Q_1)^2 \left(1 + 16D^2(\omega'_p)\right)} \times R_E \left[1 + \frac{\kappa}{\pi^2 F'_p} - \frac{4}{\pi^2 \Gamma} \kappa \left(1 + 16D^2(\omega'_p) \right) \times \left(1 + \ln\left(\frac{F'_p}{F_h} \right) \right) \right]. \quad (36)$$

By considering both $Q_1 >> 1$ and $\tau << 1$s, which corresponds to a frequency Γ much larger than the seismic frequency, the behaviour of ζ'_p with Q_2 can be approximated to:

$$\frac{\partial \zeta'_p}{\partial Q_2} \simeq \frac{-4Q_1^2}{(Q_2 - Q_1)^2 \left(1 + 16D^2(\omega'_p)\right)} R_E \left[1 + \frac{\kappa}{\pi^2 F'_p} \right]. \quad (37)$$

Since κ ranges between -1 and 1, the peak phase attribute increases or decreases monotonically with Q_2 from $\zeta'_{p\infty}$ (equation (32b)) to ζ_{p_p} (equation (30c)) when R_E is negative or positive, respectively.

References

Adam, L., Batzle, M., Lewallen, K.T. & van Wikj, K., 2009. Seismic wave attenuation in carbonates, *Journal of Geophysical Research*, **114**, B06208.

Borcherdt, R.D., 2009. *Viscoelastic Waves in Layered Media*, Cambridge University Press.

Bourbié, T. & Nur, A., 1984. Effects of attenuation on reflections: Experimental test, *Journal of Geophysical Research*, **89**, 6197–6202.

Brossier, R., 2011. Two-dimensional frequency-domain visco-elastic full waveform inversion: parallel algorithms, optimization and performance, *Computers & Geosciences*, **37**, 444–455.

Causse, E., Mittet, R. & Ursin, B., 1999. Preconditioning of full-waveform inversion in viscoacoustic media, *Geophysics*, **64**, 130–145.

Castagna, J.P., Sun, S. & Siegfried, R.W., 2003. Instantaneous spectral analysis: detection of low-frequency shadows associated with hydrocarbons, *The Leading Edge*, **22**, 120–127.

Chapman, M., Liu, E. & Li, X.-Y., 2006. The influence of fluid-sensitive dispersion and attenuation on AVO analysis, *Geophysical Journal International*, **167**, 89–105.

Chen, H., Innanen, K.A. & Chen, T., 2018. Estimating P- and S-wave inverse quality factors from observed seismic data using an attenuative elastic impedance, *Geophysics*, **83**, R173–R187.

Dasgupta, R. & Clark, R.A., 1998. Estimation of Q from surface seismic reflection data, *Geophysics*, **63**, 2120–2128.

Dutta, G. & Schuster, G.T., 2014. Attenuation compensation for least-squares reverse time migration using the viscoacoustic-wave equation, *Geophysics*, **79**, S251–S262.

Futterman, W.I., 1962. Dispersive body waves, *Journal of Geophysical Research*, **67**, 5279–5291.

Guerin, G. & Goldberg, D., 2005. Modeling of acoustic wave dissipation in gas hydrate-bearing sediments, *Geochemistry Geophysics Geosystems*, **6**, Q07010.

Gurevich, B., Osypov, K., Ciz, R. & Makarynska, D., 2008. Modeling elastic wave velocities and attenuation in rocks saturated with heavy oil, *Geophysics*, **73**, E115–E122.

Innanen, K., 2011. Inversion of the seismic AVF/AVA signatures of highly attenuative targets, *Geophysics*, **76**, R1–R14.

Innanen, K.A. & Lira, J.E., 2010. Direct nonlinear Q-compensation of seismic primaries reflecting from a stratified, two-parameter absorptive medium, *Geophysics*, **75**, V13–V23.

Ker, S., Le Gonidec, Y. & Gibert, D., 2012. Multiscale seismic attributes: source-corrected wavelet response and application to high-resolution seismic data, *Geophysical Journal International*, **190**, 1746–1760.

Ker, S., Le Gonidec, Y., Marsset, B., Westbrook, G., Gibert, D. & Minshull, T.A., 2014. Fine-scale gas distribution in marine sediments assessed from deep-towed seismic data, *Geophysical Journal International*, **196**, 1466–1470.

Ker, S., Thomas, Y., Riboulot, V., Sultan, N., Bernard, C., Scalabrin, C., Ion, G. & Marsset, B., 2019. Anomalously deep BSR related to a transient state of the gas hydrate system in the Western Black Sea, *Geochemistry Geophysics Geosystems*, **20**, 442–459.

Kjartansson, E., 1979. Constant Q-wave propagation and attenuation, *Journal of Geophysical Research*, **84**, 4737–4748.

Kolsky, H., 1956. The propagation of stress pulses in viscoelastic solids, *Philosophical Magazine*, **1**, 693–710.

Lam, C.-H., Kooij, B.J. & De Hoop, A.T., 2004. Impulsive sound reflection from an absorptive and dispersive planar boundary, *Journal of the Acoustical Society of America*, **116**, 677–685.

Li, Q., Zhou, H., Zhang, Q., Chen, H. & Sheng, S., 2016. Efficient reverse time migration based on fractional Laplacian viscoacoustic wave equation, *Geophysical Journal International*, **204**, 488–504.

Lines, L., Vasheghani, F. & Treitel, S., 2008. Reflections on Q, *CSEG Recorder*, **December**, 36–38.

Lines, L., Wong, J., Innanen, K., Vasheghani, F., Sondergeld, C., Treitel, S. & Ulrych, T., 2014. Experimental measurements of Q-contrast reflections, *Geophysical Prospecting*, **62**, 190–195.

Marin-Moreno, H., Sahoo, S.K. & Best, A.I., 2017. Theoretical modeling insights into elastic wave attenuation mechanisms in marine pore-filling methane hydrate, *Journal of Geophysical Research: Solid Earth*, **122**, 1835–1847.

Morgan, E.C., Vanneste, M., Lecomte, I., Baise, L.G., Longva, O. & McAdoo, B., 2012. Estimation of free gas saturation from seismic reflection surveys by the genetic algorithm inversion of P-wave attenuation model, *Geophysics*, **77**, R175–R187.

Morozov, I., 2011. Anelastic acoustic impedance and the correspondence principle, *Geophysical Prospecting*, **59**, 24–34.

Odebeatu, E., Zhang, J., Chapman, M., Liu, E. & Li, X.-Y., 2006. Application of spectral decomposition to detection of dispersion anomalies associated with gas saturation, *The Leading Edge*, **25**, 206–210.

Quintal, B., Schmalholz, S.M. & Podladchikov, Y., 2009. Low-frequency reflections from a thin layer with high attenuation caused by interlayer flow, *Geophysics*, **74**, N15–N23.

Reine, C., van der Baan, M. & Clark, R., 2009. The robustness of seismic attenuation measurements using fixed- and variable-window time-frequency transforms, *Geophysics*,**74**, WA123–WA135.

Takam Takougang, E. & Bouzidi, Y., 2018. Imaging high-resolution velocity and attenuation structures from walkaway vertical seismic profile data in a carbonate reservoir using visco-acoustic inversion, *Geophysics*, **83**, B323–B337.

Tary, J.B., van der Baan, M. & Herrera, R.H., 2017. Applications of high-resolution time-frequency transforms to attenuation estimation, *Geophysics*, **82**, V7–V20.

Toksöz, M.N. & Johnston, D.H., 1981. *Seismic Wave Attenuation*. SEG, Tulsa, p. 45.

Wang, Y., 2002. A stable and efficient approach of inverse Q filtering, *Geophysics*, **67**, 657–663.

Wang, Y. & Guo, J., 2004. Modified Kolsky model for seismic attenuation and dispersion, *Journal of Geophysics and Engineering*, **1**, 187–196.

Wang, Y., 2008a. Inverse-Q filtered migration, *Geophysics*, **73**, S1–S6.

Wang, Y., 2008b. *Seismic Inverse Q Filtering*. Blackwell, Oxford.

Wang, Y., 2015a. The Ricker wavelet and the Lambert W function, *Geophysical Journal International*, **200**, 111–115.

Wang, Y., 2015b. Generalized seismic wavelets, *Geophysical Journal International*, **203**, 1172–1178.

White, J.E., 1965. Reflections from lossy media, *The Journal of the Acoustical Society of America*, **38**, 604–607.

Wu, X., Chapman, M. & Angerer, E., 2015. Interpretation of phase reversals in seismic reflections from attenuating targets, *Geophysical Journal International*, **200**, 690–697.

Zhang, Z. & Ulrych, T.J., 2002. Estimation of quality factors from CMP records, *Geophysics*, **67**, 1542–1547.

Zhao, H., Gao, J. & Peng, J., 2018. Frequency-dependent reflections in elastic diffusive-viscous media, *Journal of Geophysics and Engineering*, **15**, 1900–1916.

Zhu, T., Harris, J.M. & Biondi, B., 2014. Q-compensated reverse-time migration, *Geophysics*, **79**, S77–S87.